

This work is on a Creative Commons Attribution-NonCommercial-NoDerivatives 4.0 International license, <https://creativecommons.org/licenses/by-nc-nd/4.0/legalcode>. Access to this work was provided by the University of Maryland, Baltimore County (UMBC) ScholarWorks@UMBC digital repository on the Maryland Shared Open Access (MD-SOAR) platform.

Please provide feedback

Please support the ScholarWorks@UMBC repository by emailing scholarworks-group@umbc.edu and telling us

what having access to this work means to you and why it's important to you. Thank you.

The use of porcine corrosion casts for teaching human anatomy

Eberlova Lada^{a,b}, Liska Vaclav^{b,c}, Mirka Hynek^{b,d}, Tonar Zbynek^{b,e}, Haviar Stanislav^f, Svoboda Milos^g, Benes Jan^g, Palek Richard^{b,c}, Eminger Michal^{b,c}, Jachym Rosendorf^{b,c}, Mik Patrik^a, Sarah Leupen^h, Lametschwandtner Aloisⁱ

^a Department of Anatomy, Faculty of Medicine in Pilsen, Charles University, Karlovarska 48, 301 66 Pilsen, Czech Republic

^b Biomedical Centre, Faculty of Medicine in Pilsen, Charles University, Alej Svobody 76, 323 00 Pilsen, Czech Republic

^c Department of Surgery, University Hospital in Pilsen, Alej Svobody 80, 304 60 Pilsen, Czech Republic

^d Department of Imaging Methods, University Hospital in Pilsen, Alej Svobody 80, 304 60 Pilsen, Czech Republic

^e Department of Histology and Embryology, Faculty of Medicine in Pilsen, Charles University, Karlovarska 48, 301 66 Pilsen, Czech Republic

^f Department of Physics and NTIS – European Centre of Excellence, Faculty of Applied Sciences, University of West Bohemia, Univerzitni 22, 306 14 Pilsen, Czech Republic

^g New Technology Research Centre – CENTEM, University of West Bohemia, Univerzitni 8, 306 14 Pilsen, Czech Republic

^h Department of Biological Sciences, University of Maryland Baltimore County, 1000 Hilltop Circle, Baltimore, Maryland, 21250 USA

ⁱ Department of Cell Biology and Physiology, University Salzburg, Hellbrunner Str. 34, A-5020 Salzburg, Austria

Corresponding author: Lada Eberlova, Department of Anatomy, Faculty of Medicine in Pilsen, Charles University, Karlovarska 48, 301 66 Pilsen, Czech Republic

E-mail: lada.eberlova@lfp.cuni.cz

Tel.: +420377593302

Abstract

In teaching and learning human anatomy, anatomical autopsy and prosected specimens have always been indispensable. However, alternative methods must often be used to demonstrate particularly delicate structures. Corrosion casting of porcine organs with Biodur E20[®] Plus is valuable for teaching and learning both the gross anatomy and, uniquely, the micromorphology of cardiovascular, respiratory, digestive, and urogenital systems. Assessments of casts with a stereomicroscope and/or scanning electron microscope as well as highlighting cast structures using color coding helps students to better understand how the structures that they have observed as two-dimensional images actually exist in three dimensions. Reconstructions of cast hollow structures from (micro-)computed tomography scans and videos facilitate detailed analyses of branching patterns and spatial arrangements in cast structures, aid in the understanding of clinically relevant structures and provide innovative visual aids. The casting protocol and teaching manual we offer can be adjusted to different technical capabilities and might also be found useful for veterinary or other biological science classes.

Key words

corrosion casting; anatomy; Biodur E20[®] Plus; microcomputed tomography; pig

Abbreviations

CC, corrosion cast

1. Introduction

Corrosion casting is a longstanding method used to visualize the morphology of hollow structures. It is based on the filling the cavity with solidifying material, after which the surrounding tissue is removed with use of a corrosion agent after its polymerization. Although the first attempts are often attributed to Leonardo da Vinci (Hermiz et al., 2011; De Sordi et al., 2014), who filled the ox brain ventricles with wax and scraped the overlying tissue off (Paluzzi et al., 2007) between 1504 and 1507, casting was performed earlier and can be divided into the “pre” and “corrosion” periods (Aharinejad and Lametschwandtner, 1992a). The oldest recorded attempts to fill the human blood vessels date back to 14th century and Alessandra Giliani (1307–1326), the first woman anatomist and prosector, professor of medicine at the University of Bologna. Giliani developed a technique to make blood vessels visible by filling them with colored, hardening liquids. However, the first notes of injection of a solidifying material followed by parenchymal corrosion were recorded by Dutch anatomist Govert Bidloo (1649–1713), the author of the anatomical atlas *Anatomia Humani Corporis*, who used melted metal to inject trachea and bronchi and boiled the specimen to remove connective tissues (Davies, 1973). Since then, casting materials and procedures have been gradually improved. At present, the casting media available which are suitable for corrosion range from low-viscosity, hard and brittle materials, such as methyl methacrylates, to pliable thermostable polyurethanes or epoxy resins to flexible silicone rubber (Haensgen et al., 2014, Table 1). Each of the agents has its pros and cons, and choosing the optimal one is always a balance between the research purpose and the specimen quality. For example, for the high volume vascular corrosion casts a resin with a sufficient processing time must be chosen. And if we intend to examine the cast with the use of X-ray, the resin must be also radiopaque. Since the 1960s, corrosion casts (CCs) have been studied using light microscopy.

Nowell et al. (1971) and Murakami (1971) first applied scanning electron microscopy (SEM) in CC assessment. With recent advances in high-resolution computed tomography (CT) technology, a pixel resolution close to 1 μm allows for morphometry of microvessels comparable with classical light microscopy. CC $\mu\text{-CT}$ scanning provides new data from the microvascular tree that can be used both for the mathematical modeling (Debbaut et al., 2014) or quantitative purposes (Jiřík et al., 2016).

CCs enable the study of three-dimensional (3-D) arrangement of (micro)vascular systems, including angiogenesis (Gerlach et al., 2014). In combination with SEM, vascular CCs provide information about structures that protrude from the wall and cause imprints, e.g., the endothelial cell nuclei, valves, and constrictions. These replicates help to differentiate arterial from venous vessels (Miodonski et al., 1976) and to identify different parts of the vascular bed (Lametschwandtner and Lametschwandtner, 1990; Aharinejad and Lametschwandtner, 1992).

Our goal at the very beginning was purely scientific – we needed to obtain three-dimensional data of human liver microvasculature for mathematical modeling of the blood perfusion. Due to ethical concerns and the practical impossibility of obtaining fresh and healthy human livers, we focused on the use of porcine livers. Given its size, morphology and function, the porcine liver is frequently used as a large-animal liver model, e.g., for testing surgical techniques (Bedoya et al., 2014), liver transplantation (Okada et al., 2015), regeneration (Mortensen and Revhaug, 2011; Avritscher et al., 2013), mathematical modeling (Fu and Chui, 2014), gene therapy (Carreño et al., 2013) and pharmacology (Gnutzmann et al., 2015). After testing different resins, we optimized the protocol of hepatectomy and high-volume corrosion casting with Biodur E20[®] Plus (Eberlova et al., 2015). Of all resins tested, Biodur E20[®] Plus (Biodur products, Heidelberg, Germany) exhibited the best handling qualities: it passes with minimal leakage through the capillaries, its processing time enables the high volume filling, it is

slightly flexible and alcohol resistant after hardening, and it is radio-opaque. Because of the high quality and high teaching potential of the resulting preparations as well as easy organ accessibility—pigs are bred in our biomedical center and are sacrificed for a variety of research topics—we decided to prepare other parenchymal organs that otherwise would be wasted for use in teaching anatomy.

The aims of our study were 1. to evaluate the suitability of Biodur E20[®] Plus porcine corrosion casts for teaching human anatomy; 2. to enhance students' understanding of macro- and microvascular structures of clinical relevance; 3. to interconnect the macro- with the microanatomy with cast assessment by light microscopy and scanning electron microscopy; 4. to create original, innovative visual aids useful for lectures and projections.

2. Methods and results

The experimental surgical and anesthesia procedures and the use of piglets in this study were certified by the Commission for Work with Experimental Animals at the Pilsen Medical Faculty of Charles University, Prague, and were under the control of the Ministry of Agriculture of the Czech Republic. All procedures were prepared and performed under the law of the Czech Republic, which is compatible with the legislation of the European Union.

2.1 Surgery

The detailed protocols for surgery and casting were published by Eberlova et al. (2015). Briefly, healthy Prestice Black-Pied pigs (Vrtkova, 2015), N = 7, age 16 to 18 weeks, weight 35 to 45 kg, both sexes, were premedicated, and intravenous anesthesia was administered continuously. For organs cast, see Table 2. After myorelaxation, the pigs were intubated and mechanically ventilated. Heparin (30,000 UI i.v.) and volume-substituting infusions were administered. Before hepatectomy, the vascular bed of the liver was flushed with 5 L of

heparinized (10,000 I.U.) Hartmann's solution administered via a tube inserted into the suprahepatic portion of the caudal caval vein. Then, the organ under consideration was disconnected from blood circulation and the vascular tree of liver, kidney and/or spleen was flushed with heparinized solution (dilution 10,000 UI of heparin per 1 L of cold Hartmann's solution) via the suprahepatic portion of the inferior caval vein (liver), renal arteries (kidney) or splenic artery (spleen). The hepatic portal vein (PV) and hepatic artery (HA) or renal veins or splenic vein remained unligated to drain the perfused solution. The bronchial tree was harvested together with the lungs.

2.2 *Casting procedure*

All vessels were cannulated while submerged in water to prevent aspiration of air into vessels. Biodur E20[®] (Biodur Products, Heidelberg, Germany) for injection was mixed at a ratio of 100 g Biodur E20[®] Plus/45 g of catalyst E2(0). The PV was filled using manual injection pressure. For injecting the hepatic, splenic and renal arteries, the cannula was held and guided by a micromanipulator (Aharinejad and Lametschwandtner, 1992b). After filling specimens were submerged in tap water (20°C; 24 hours) for hardening, they were transferred to 15% potassium hydroxide for tissue removal (40°C; 2–3 days), rinsed in tap water, and either stored in 70% denatured alcohol or, for higher resolution imaging, frozen in distilled water to be subsequently cut into ice cubes (approximately 2 cm x 1 cm x 1 cm) with a belt saw.

2.3 *Scanning and data processing*

Although even the gross CC can be very educative (Fig. 1)—the students can see the nature and density of the vasculature even with the naked eye—various devices can be used to see the details of the vascular tree. The liver CC owing to its size can be examined with the

common multi-slice human CT scanner (Fig. 2A), and any cast can be examined with a stereomicroscope (Fig. 3C, D).

To provide the students morphological details in ascending resolution, our casts were analyzed first with the **stereomicroscope** (Olympus SZX7; Tokyo, Japan). Liver casts were then scanned in 90% denatured alcohol (provides higher contrast than water) with a **multi-slice human CT scanner** (Somatom Sensation64, Siemens, Forchheim, Germany; slice thickness: 0.6 mm; voxel size: 4 x 0.4 x 0.6 mm). For high-resolution imaging, a lobe (liver) or lobule (bronchial tree) was dissected, whereas whole kidneys or spleens were frozen in distilled water and randomly cut with a belt saw into pieces (size ~2 x 1 x 1 cm). Randomly chosen prisms were then immersed in 5% formic acid for 5 min (Lametschwandtner et al., 1990), rinsed in distilled water, air dried, mounted, sputter-coated with gold (1 min) and examined by the **scanning electron microscope** in a Stereoscan 250 instrument (Cambridge, UK) at 10 kV or in a SU-70 (Hitachi, Japan) at 1 kV accelerating voltage (Fig. 4, 5B).

Liver casts were scanned in air with a **μ -CT scanner** (Xradia μ XCT 400, Pleasanton, CA, USA). Samples were first scanned using the Macro detector (pixel size: 47 μ m/px, 1024x1024 px resolution) to display the overall liver cast structure. Then, the most interesting parts were scanned again with a high-resolution detector using the following parameters: source voltage 40 kV, source power 4 W, pixel size 4.1 μ m, detector resolution 1024 x 1024 pixels (binning 2), rotation angle 360°, number of images 1500, overall scanning time 3 hours, and temperature 28°C. After scanning, recorded images were used for 3-D reconstruction using specialized software supplied with the Xradia machine. Then, reconstruction scans were filtered and semi-automatically segmented using the software Avizo 7.2 (vsg) and FIJI ImageJ 1.50f (National Institutes of Health, USA). Salt-and-pepper noise was removed by filtering. Image segmentation was performed by thresholding and manually controlled flooding. Skeletonization was used to extract topological information (Fig. 2 B, D, video).

For the 3-D reconstructions and brief data processing, the data from μ -CT scanner can be used for the volume rendering technique and thin-slab maximum intensity projection, software commonly available in human CT-scanners (Fig. 2C).

2.4 Use of corrosion casting in elective anatomical classes – the schedule

Basic knowledge of general anatomy and histology were prerequisites to be accepted for elective anatomical classes. The schedule for the second-year medical students (Table 3) is outlined below: **Week 1:** In collaboration with surgeons, the instructors obtain a fresh organ that is immediately cannulated and injected with resin as described in the Materials and Methods. Students only watch the procedure, which is performed by an instructor, and wear protective glasses. The room is ventilated to prevent exposing students and staff to toxic fumes. The injected organ is left submerged in tap water for approximately 24 hours at 20°C for hardening. In the next 3 days, the organ is macerated (corroded) and rinsed in running tap water. **Week 2:** Students inspect casts with the stereomicroscope and select the part of the cast they want to analyze in the SEM. This part is frozen in distilled water and cut into $\sim 1 \text{ cm}^3$ ice cubes. Ice cubes are allowed to thaw in distilled water, and casts are cleaned from any debris under binocular control (Lametschwandtner et al., 1990). Clean casts are then placed onto filter paper and air dried. **Week 3:** Students are introduced to theoretical principles of SEM and prepare specimens for SEM observation, i.e., mount dry casts onto specimen stubs and sputter-coat specimens with gold. Finally, students together with the instructor watch images of selected areas of vascular casts on the SEM display and discuss the displayed structures in terms of cast quality, vascular patterns, normal versus pathological, or real structure versus artifact (Fig. 6).

2.5 Useful tips for easy teaching

- Highlight cast structures by **color-coding**, e.g., using differently colored Biodur E20[®] Plus for arteries (e.g., red Biodur) and veins (e.g., blue Biodur). It enables the ability to distinguish the two vascular beds (**Fig. 1, 3**). For this purpose, either the colored Biodur E20[®] dye can be used, or the clear Biodur E20[®] can be dyed with different dye pastes.
- As the fresh organs are not always available, an organ filled with Biodur E20[®] can be stored in 50% alcohol and corroded later.
- It is also useful for the anatomy classes for the instructor to demonstrate the vascular density showing the students the organ before and after corrosion (Fig. 1A, B).
- Looking at the CCs, students do not often understand what they see. The instructor should ask questions dealing with the structures on the cast to train the students' imagination; point out that there is not any soft tissue present and that the students are seeing the filling of the former vessels (cavities); and relate the corrosion casts to clinical conditions (for example, the instructor can ask students how the cast would look different in a cirrhotic liver).

3. Discussion

In teaching anatomy, the importance and merit of anatomical autopsy have not been and probably will not be overcome in the near future. Nevertheless, prosected specimens do not always provide the student with a clear picture of particular, delicate anatomical structures. This gap can be partly bridged by corrosion casts, which represent a 3-D replica of hollow structures. As CCs represent real specimens, they support the learning process considerably more than textbooks or even computer-based 3-D models (Preece et al., 2013).

The idea of engaging students in active learning by letting them work with CCs is not new; CCs of bronchial trees have been used in class (Cope, 2007; Hermiz et al., 2011; De Sordi et al., 2014). However, given that casting media were too viscous and did not fill tiny spaces, the casts only exhibited gross structures, such as the basic branching pattern, and they lacked

detailed information on the terminal tree (Klaws and Tillmann, 1993). In contrast, Biodur E20[®] Plus passes through capillary-sized tubes and can fill (cast) large-sized spaces (high volume filling). This resin is a two-component, temperature-tolerant and chemically resistant resin that is suitable both for freezing and corrosion. It is relatively cheap (Table 1) and suitable for macro- and μ -CT scanning (Figs. 2 and 4). Its slightly flexible consistency is also advantageous for comfortable handling and demonstration purposes compared with brittle, quickly hardening casting materials (Haensgenn et al., 2014). After solidifying, casts made from Biodur E20[®] can also be stored in alcohol to prolong the precorrosion period. Alcohol preservation is also useful for voluminous corroded CCs to prevent them from molding. An additional advantage of using this method of corrosion casting is that highlighting cast structures by color-coding, e.g., using differently colored Biodur E20[®] Plus for arteries (e.g., red Biodur) and veins (e.g., blue Biodur), enables the ability to distinguish the two vascular beds and casts assessment by the dissecting microscope and allows the visualization of arteriovenous anastomosis (AV shunts, Fig. 3D).

3.1 Porcine liver corrosion casts

When teaching human anatomy with porcine corrosion casts, the morphological similarities and dissimilarities in the cast organs compared to their human counterparts must be taken into consideration (Tables 4 and 5). Regarding external morphology, the right and left hemilivers in pigs are separated by a deep fissure, and only five lobes are invariably present: the left lateral, left medial, right lateral, right medial and the caudate lobes (Court et al., 2003). The quadrate lobe is present occasionally (Fig. 5B and D). Nevertheless, given the similarity of the vascular and biliary tree, the eight segments in the parenchyma are present and are roughly similar to those described in the human by Couinaud (Couinaud, 1954, Court et al., 2003). Microscopically, porcine liver lobules are clearly demarcated by the interlobular connective

tissue septa that meet in the portal area. In healthy humans, liver lobules normally lack connective tissue, the presence of connective tissue, which departs from the portal areas indicates liver fibrosis or cirrhosis (Hytioglou, 2011). Similar to the human liver, the interlobular space in the porcine liver is occupied by the portal triad. The interlobular hepatic artery and portal vein open into sinusoids, which empty into the central vein (Fig. 4A).

Using the CCs enables to demonstrate the difference between portal vein and hepatic artery perfusion (Fig. 1A and C). The hepatic artery exclusively supplies three compartments: the peribiliary vascular plexus (Ohtani et al., 1982; Fig. 4 B), the portal tract interstitium and the portal vein wall (Elias and Petty, 1953; Fig. 1 C). Detailed knowledge of the anatomy of the biliary pathways blood supply is crucial not only for cholecystectomies but also for liver transplantations, as the bile ischemia is believed to be the major factor of biliary complications (Wang et al., 2015).

Our liver CCs clearly demonstrate also the vasa vasorum (Fig. 1 C). Vasa vasorum play a crucial role in vascular pathologies (Mulligan-Kehoe and Simons, 2014; Tonar et al., 2016), especially in atherosclerosis (Xu et al., 2015).

Macro-CT of liver vascular CC applies clinical imaging in the teaching of anatomy (Fig. 2A). CT scans enable the differentiation of vessels with a lumen diameter as small as 3 mm. Similarly, μ -CT and 3-D reconstruction visualize the branching and spatial arrangement of the microvascular tree (Fig. 2B–D, video). Tracing the vessels may reveal the presence of intrahepatic porto-systemic anastomoses (PS shunts; Fig. 2C). Although the PS shunts are only sporadically noted within the human liver parenchyma (Palvanov et al., 2016), the extrahepatic porto-caval anastomoses (PC shunts) are relevant structures in human medicine and play an extremely important role in case of the portal hypertension. PC shunts are found in the rectum, esophagus, abdominal wall, and retroperitoneum. They are valveless and serve as bypasses that open in case that the blood can not flow through the liver. When the large

volume of blood circumvents the liver, varicose veins develop at the sites of porto-systemic anastomoses. They protrude, may rupture and, in combination with the lack of coagulation proteins caused by the accompanied hepatopathy, cause life-threatening bleeding.

3.2 *Spleen, kidney and bronchial tree corrosion casts*

With respect to shape and position, the kidney is one of the most variable organs in humans. The prevalence of vascular variations is high (Çınar and Türkvatan, 2016). Nevertheless, there are many similarities between the human and pig kidney (Table 5), e.g., in parenchyma stratification, microangioarchitecture, and nephron morphology (Friis 1980). The porcine kidney is a widely used animal model in experimental medicine (Tonar et al., 2009, Nath et al., 2014, Yang et al., 2015). The adult organ has a similar weight, size and number of nephrons as that in humans (Rytand, 1938). Of note, there are 4 renal segments in pigs. In 91 % of pigs, the renal artery bifurcates at or before the hilus into upper and lower polar arteries, each of which branches off into an anterior and a posterior segmental artery. The avascular plane is transverse in swine (Evan et al., 1996) but longitudinal in humans (Dyer et al., 2002). Pig kidney vascular CCs clearly demonstrate the difference between the texture of the cortex and medulla. The dotted cortex contains the glomeruli, whereas the striped medulla contains the straight arterioles. The outlines of renal pyramids are also distinct (Fig. 3B, C). The ureteric branches supplying the renal pelvis and upper ureter are clearly visible in the casts filled via the renal artery (Fig. 3A).

Similar size and anatomy to the human lung make the pig lung a beneficial model for biomedical research (Nishikawa et al., 2013; Judge et al., 2014; Meyerholz, 2016). The lobar anatomy in pigs is similar to that of the human left lung, which consists of cranial and caudal lobes. The right lung is divided into four lobes: the cranial, middle, accessory and caudal. Interlobar fissures are incomplete. The right cranial lobar bronchus arises directly from the

lateral wall of the trachea, whereas the other lobar bronchi ramify from the main bronchi at the hilum. In the pig, the segmentation and bronchial ramification is more indented compared with humans, e.g., the left caudal lobar bronchus divides into 4 ventral and 4 dorsal segmental bronchi (Nakakuki, 1994). Porcine airways are more cartilaginous but exhibit similar bronchial generations (N = 23) compared with humans (Maina and Gils, 2001). In contrast to humans, the porcine branching pattern is monopodial (Noble et al., 2010). In addition, the secondary lobules are completely separated by connective tissue septa, i.e., they are clearly demarcated in the CC after soft tissue digestion. Towards the periphery, the respiratory bronchioles give rise to alveolar ducts that end in alveoli (Fig. 4C, D).

The shape of the porcine spleen is significantly different from the human spleen. Spleens obtained from our Prestice Black-Pied pigs aged 16 to 18 weeks were approximately 20 cm long and 6 cm wide (Fig. 5A). The splenic artery divides close to the hilum into 2 segmental branches, which supply two independent splenic segments (Pereira-Sampaio and Marques-Sampaio, 2006). According to a Web of Science search (September 2016, key words “pig spleen histology”), the ultrastructure of the porcine spleen was studied mainly in connection with experiments and histopathology (Palzer et al., 2015; Suzuki et al. 2016). To understand the spleen’s functions, it is important to have knowledge of the 3-D structure of the microvasculature, the tissue compartments and the cell distribution. Given that mammalian spleens have an open circulation, corrosion casting is not an ideal method for studying the red pulp. Nevertheless, in the white pulp Biodur E20[®] CCs clearly demonstrate the central and penicillar arteries and indicate the presence of the periarteriolar lymphoid sheaths (Fig. 5B).

4. Conclusions

Pigs are frequently used as large-animal models. Corrosion casts of porcine organs with Biodur E20[®] Plus appeared to be valuable for teaching human anatomy of cardiovascular,

respiratory, digestive, and urogenital systems. We present a manual for the corrosion casting and the cast analysis in the elective anatomical classes. Our casting protocol and the range of CC assessment offer different variations adjustable to the particular technical demands. Biodur E20[®] passes through capillary-sized tubes and enables both gross anatomy and microstructural research. Highlighting structures using different color-coded Biodur allows for a clear demonstration of gross arterial supply and venous drainage as well as different kinds of anastomosis and microvascular patterns. Assessments of casts enable instructors to demonstrate particular structures of clinical importance, using a stereomicroscope and/or scanning electron microscope together with 3-D reconstructions based on CT scans. They also enable the creation of original visual aids, and involves the students directly in the active learning process, helping them to better understand 2-D images they know from textbooks or histological specimens. Finally, Biodur E20[®] Plus corrosion casting might be a valuable teaching tool also in veterinary anatomy or other biological science classes.

Conflict of interest statement

There are none.

Role of funding source

This study was supported by Ministry of Education Youth and Sports of the Czech Republic and the National Sustainability Programme [Grant Numbers LO1503, CENTEM CZ.1.05/2.1.00/03.0088, CENTEM PLUS (LO1402)]; Charles University in Prague [Grant Numbers SVV 260284, IP 2016–18].

Acknowledgements

Many thanks to Dr. Örs Petnehazy, Ph.D. for sharing their valuable experience.

References:

- Aharinejad, S.H., Lametschwandtner, A., 1992. Microvascular Corrosion Casting in Scanning Electron Microscopy, first edition. Springer, Berlin-Heidelberg-Wien, pp. 3–9 (a), pp. 58 (b)
- Avritscher, R., Abdelsalam, M.E., Javadi, S., Ensor, J., Wallace, M.J., Alt, E., Madoff, D.C., Vykoukal, J.V., 2013. Percutaneous intraportal application of adipose tissue-derived mesenchymal stem cells using a balloon occlusion catheter in a porcine model of liver fibrosis. *J Vasc Interv Radiol.* 24:1871–8.
- Bedoya, M., del Rio, A.M., Chiang, J., Brace, C.L., 2014. Microwave ablation energy delivery: influence of power pulsing on ablation results in an ex vivo and in vivo liver model. *Med Phys.* 41:123301.
- Carreño, O., Sendra, L., Montalvá, E., Miguel, A., Orbis, F., Herrero, M.J., Noguera, I., Aliño, S.F., Lopez-Andujar, R., 2013. A surgical model for isolating the pig liver in vivo for gene therapy. *Eur Surg Res.* 51:47–57.
- Christo, M.C., DiDio, L.J., 1997. Anatomical and surgical aspects of splenic segmentectomies. *Ann. Anat.* 179:461–74.
- Çınar, C., Türkvatan, A., 2016. Prevalence of renal vascular variations: Evaluation with MDCT angiography. *Diagn Interv Imaging.* 97:891–7.
- Cope, L.A., 2008. Tracheobronchial cast production and use in an undergraduate human anatomy course. *Anat Sci Educ.* 1:23–6.
- Couinaud, C., 1954. Liver lobes and segments: notes on the anatomical architecture and surgery of the liver. *Presse Med.* 62:709–12.
- Court, F.G., Wemyss-Holden, S.A., Morrison, C.P., Teague, B.D., Laws, P.E., Kew, J., Dennison A.R., Maddern, G.J., 2003. Segmental nature of the porcine liver and its potential as a model for experimental partial hepatectomy. *Br J Surg.* 90:440–4.
- Davies, A., 1973. The evolution of bronchial casts. *Med Hist.* 17:386–91.
- De Sordi, N., Bombardi, C., Chiocchetti, R., Clavenzani, P., Trerè, C., Canova, M., Grandis, A., 2014. A new method of producing casts for anatomical studies. *Anat Sci Int.* 89:255–65.
- Debbaut, C., Segers, P., Cornillie, P., Casteleyn, C., Dierick, M., Laleman, W., Monbaliu, D., 2014. Analyzing the human liver vascular architecture by combining vascular corrosion casting and micro-CT scanning: a feasibility study. *J. Anat.* 224:509–17.
- Dyer, R.B., Regan, J.D., Kavanagh, P.V., Khatod, E.G., Chen, M.Y., Zagoria, R.J., 2002. Percutaneous nephrostomy with extensions of the technique: step by step. *Radiographics.* 22:503–25.
- Eberlova, L., Liska, V., Mirka, H., Gregor, T., Tonar, Z., Palek, R., Skala, M., Bruha, J., Vycital, O., Kalusova, K., Haviar, S., Kralickova, M., Lametschwandtner, A., 2015. Porcine liver vascular bed in Biodur E20 corrosion casts. *Folia Morphol. (Warsz).* 75:154–161.
- Elias, H., Petty, D., 1953. Terminal distribution of the hepatic artery. *Anat. Rec.* 116:9–17.
- Evan, A.P., Connors, B.A., Lingeman, J.E., Blomgren, P., Willis, L.R., 1996. Branching patterns of the renal artery of the pig. *Anat. Rec.* 246:217–23.
- Friis, C., 1980. Postnatal development of the pig kidney: ultrastructure of the glomerulus and the proximal tubule. *J. Anat.* 130:513–26.
- Fu, Y.B., Chui, C.K., 2014. Modelling and simulation of porcine liver tissue indentation using finite element method and uniaxial stress-strain data. *J Biomech.* 47:2430–5.
- Gerlach, N., Minnich, B., Lametschwandtner, A., 2014. Microvascularization and histomorphology of lateral line organs in adult *Xenopus laevis*. *J. Morphol.* 275:497–503.

- Gnutzmann, D.M., Mechel, J., Schmitz, A., Köhler, K., Krone, D., Bellemann, N., Gockner, T.L., Mokry, T., Kortés, N., Sommer, C.M., Kauczor, H.U., Radeleff, B.A., Stampfl, U., 2015. Evaluation of the plasmatic and parenchymal elution kinetics of two different irinotecan-loaded drug-eluting embolics in a pig model. *J Vasc Interv Radiol.* 26:746–54.
- Haenssger, K., Makanya, A.N., Djonov, V., 2014. Casting materials and their application in research and teaching. *Microsc. Microanal.* 20:493–513.
- Hermiz, D.J., O'Sullivan, D.J., Lujan, H.L., DiCarlo, S.E., 2011. Constructivist learning of anatomy: gaining knowledge by creating anatomical casts. *Anat Sci Educ.* 4:98–104.
- Hytiroglou, P., 2011. Hepatitis C. In: Saxena, R. (Ed.). *Practical Hepatic Pathology, a Diagnostic Approach.* Elsevier Saunders, Philadelphia, pp. 229–231.
- Jirík, M., Tonar, Z., Králíčková, A., Eberlová, L., Mírka, H., Kochová, P., Gregor, T., Hošek, P., Svobodová, M., Rohan, E., Králíčková, M., Liška, V., 2016. Stereological quantification of microvessels using semiautomated evaluation of X-ray microtomography of hepatic vascular corrosion casts. *Int J Comput Assist Radiol Surg.* 11:1803–19.
- Judge, E.P., Hughes, J.M., Egan, J.J., Maguire, M., Molloy, E.L., O'Dea, S., 2014. Anatomy and bronchoscopy of the porcine lung. A model for translational respiratory medicine. *Am. J. Respir. Cell Mol. Biol.* 51:334–43.
- Klavs, G.R., Tillmann, B., 1993. From the specimen workstation. Injection of synthetic materials of arteries using a four color technique--with an example of head and neck blood vessels. *Ann. Anat.* 175:221–4.
- Lametschwandtner, A., Lametschwandtner, U., Weiger, T., 1990. Scanning electron microscopy of vascular corrosion casts--technique and applications: updated review. *Scanning Microsc.* 4:889–940.
- Maina, J.N., van Gils, P., 2001. Morphometric characterization of the airway and vascular systems of the lung of the domestic pig, *Sus scrofa*: comparison of the airway, arterial and venous systems. *Comp. Biochem. Physiol., Part A Mol. Integr. Physiol.* 130:781–98.
- Mortensen, K.E., Revhaug, A., 2011. Liver regeneration in surgical animal models - a historical perspective and clinical implications. *Eur Surg Res.* 46:1–18.
- Mulligan-Kehoe, M.J., Simons, M., 2014. Vasa vasorum in normal and diseased arteries. *Circulation.* 129:2557-66.
- Murakami, T., 1971. Application of the scanning electron microscope to the study of the fine distribution of the blood vessels. *Arch Histol Jpn.* 32:445–54.
- Nakakuki, S., 1994. Bronchial tree, lobular division and blood vessels of the pig lung. *J. Vet. Med. Sci.* 56:685–9.
- Nath, J., Guy, A., Smith, T.B., Cobbold, M., Inston, N.G., Hodson, J., Tennant, D.A., Ludwig, C., Ready, A.R., 2014. Metabolomic perfusate analysis during kidney machine perfusion: the pig provides an appropriate model for human studies. *PLoS ONE* 9:e114818.
- Nishikawa, H., Oto, T., Otani, S., Harada, M., Iga, N., Miyoshi, K., Miyoshi, S., 2013. Unilateral lung transplantation using right and left upper lobes: an experimental study. *J. Thorac. Cardiovasc. Surg.* 146:1534–7.
- Noble, P.B., McLaughlin, R.A., West, A.R., Becker, S., Armstrong, J.J., McFawn, P.K., Eastwood, P.R., Hillman, D.R., Sampson, D.D., Mitchell, H.W., 2010. Distribution of airway narrowing responses across generations and at branching points, assessed in vitro by anatomical optical coherence tomography. *Respir. Res.* 11:9.
- Nowell, J.A., Tyler, W.S., 1971. Scanning electron microscopy of the surface morphology of mammalian lungs. *Am. Rev. Respir. Dis.* 103:313–28.
- Ohtani, O., Murakami, T., Jones, A.L., 1982. Microcirculation of the liver, with special reference to the peribiliary portal system. In: Motta, P.M., DiDio, L.J.A. (Eds). *Basic and Clinical Hepatology.* Martinus Nijhoff Publishers, Hague / Boston / London, pp. 85–96.

- Okada, N., Mizuta, K., Oshima, M., Yamada, N., Sanada, Y., Ihara, Y., Urahashi, T., Ishikawa, J., Tsuji, T., Hishikawa, S., Teratani, T., Kobayashi, E., 2015. A novel split liver protocol using the subnormothermic oxygenated circuit system in a porcine model of a marginal donor procedure. *Transplant. Proc.* 47:419–26.
- Palvanov, A., Marder, R.L., Siegel, D., 2016. Asymptomatic Intrahepatic Portosystemic Venous Shunt: To Treat or Not To Treat? *Int. J. Angiol.* 25:193–8.
- Palzer, A., Austin-Busse, R.L., Ladinig, A., Balka, G., Zoels, S., Ritzmann, M., 2015. Histopathologic lesions in conventional pigs experimentally infected with *Haemophilus parasuis* serovar 5. *Tierarztl Prax Ausg G Grosstiere Nutztiere.* 43:91–6.
- Pereira-Sampaio, M.A., Marques-Sampaio, B.P., 2006. Anatomical study and proportional analysis of the pig spleen arterial segments. *Cells Tissues Organs.* 182:32–4.
- Preece, D., Williams, S.B., Lam, R., Weller, R., 2013. "Let's get physical": advantages of a physical model over 3-D computer models and textbooks in learning imaging anatomy. *Anat Sci Educ.* 6:216–24.
- Rytand, D.A., 1938. The number and size of mammalian glomeruli as related to kidney and to body weight, with methods for their enumeration and measurement. *Am J Anat.* 62:507–520.
- Suzuki, R., Shin, D., Richards-Kortum, R., Coghlan, L., Bhutani, M.S., 2016. In vivo cytological observation of liver and spleen by using high-resolution microendoscopy system under endoscopic ultrasound guidance: A preliminary study using a swine model. *Endosc Ultrasound.* 5:239–42.
- Tonar, Z., Janáček, J., Nedorost, L., Grill, R., Báca, V., Zátura, F., 2009. Analysis of microcracks caused by drop shatter testing of porcine kidneys. *Ann. Anat.* 191:294–308.
- Tonar, Z., Tomášek, P., Loskot, P., Janáček, J., Králíčková, M., Witter, K., 2016. Vasa vasorum in the tunica media and tunica adventitia of the porcine aorta. *Ann. Anat.* 205:22–36.
- Twelves, D., Nerurkar, A., Osin, P., Ward, A., Isacke, C.M., Gui, G.P., 2012. The anatomy of fluid-yielding ducts in breast cancer. *Breast Cancer Res. Treat.* 132:555–64.
- Vrtková, I., 2015. Genetic admixture analysis in Prestice Black-Pied pigs. *Arch. Anim. Breed.* 58:115–151.
- Wang, J.Z., Liu, Y., Wang, J.L., Lu, L., Zhang, Y.F., Lu, H.W., Li, Y.M., 2015. Sequential vs simultaneous revascularization in patients undergoing liver transplantation: A meta-analysis. *World J. Gastroenterol.* 21:7036–46.
- Xu, J., Lu, X., Shi, G.P., 2015. Vasa vasorum in atherosclerosis and clinical significance. *Int J Mol Sci.* 16:11574–608.
- Yang, H., Weng, G., Yao, X., Tang, C., Shan, Y., 2015. Arterial Injury during Percutaneous Nephrostomy: Angiography Findings from an Isolated Porcine Kidney Model. *Urol J.* 12:2396–9.
- Zacharoulis, D., Poultsidis, A., Katsogridakis, E., Kalala, F., Nakou, M., Chatzitheofilou, C., 2008. Radiofrequency-assisted partial splenectomy: Histopathological and immunological assessment of the splenic remnant in a porcine model. *Surg Endosc.* 22:1309–16.

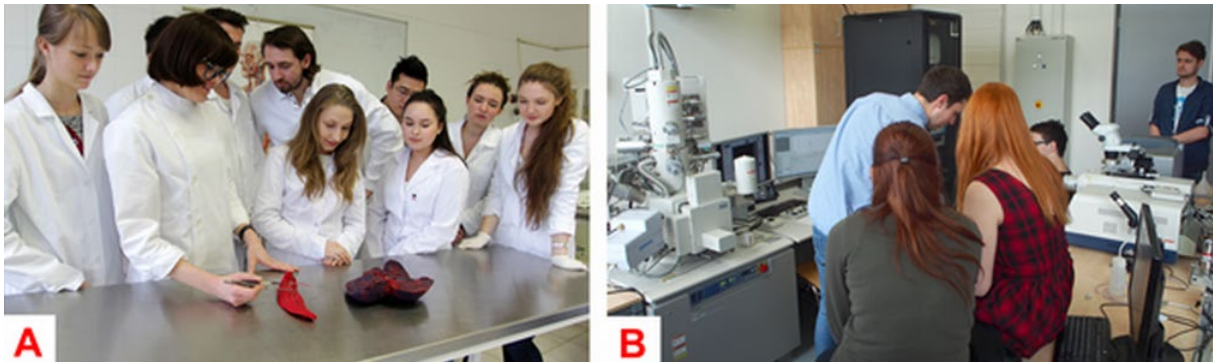


Fig. 6.

Teaching gross anatomy with porcine corrosion casts (A) and elective anatomy classes at the SEM (B).

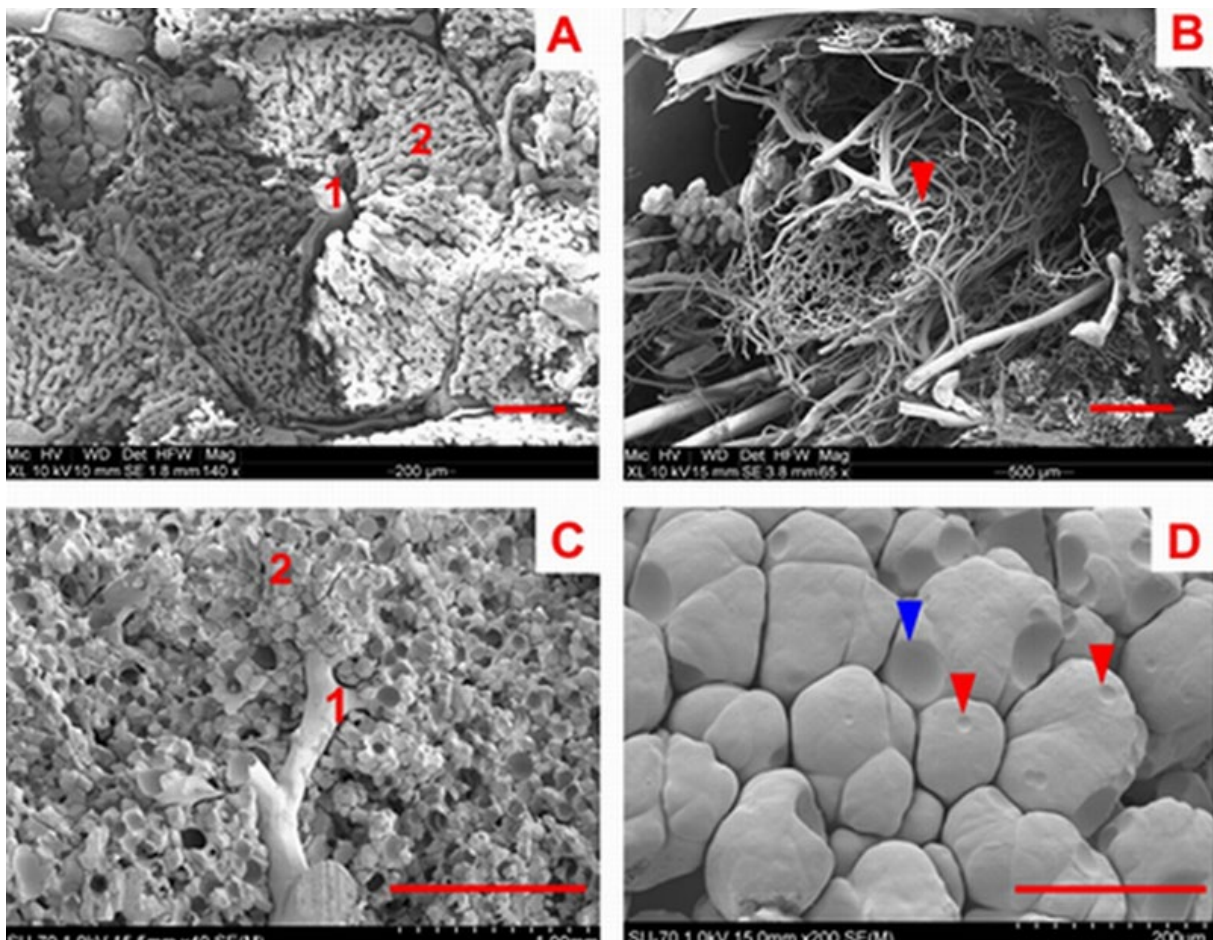


Fig. 4.

Vascular corrosion casts of porcine liver and lung. SEM. (A) Liver lobule. Central vein (1), sinusoids (2). (B) Peribiliary plexus (arrowhead). (C) Terminal bronchiole (1) and alveoli (2) of lung. (D) Pulmonary alveoli. Note nuclear imprints of pneumocytes (red arrowheads) and air bubble (blue arrowhead). Bar scale 200 μm (A), 500 μm (B), 1 mm (C), 200 μm (D).

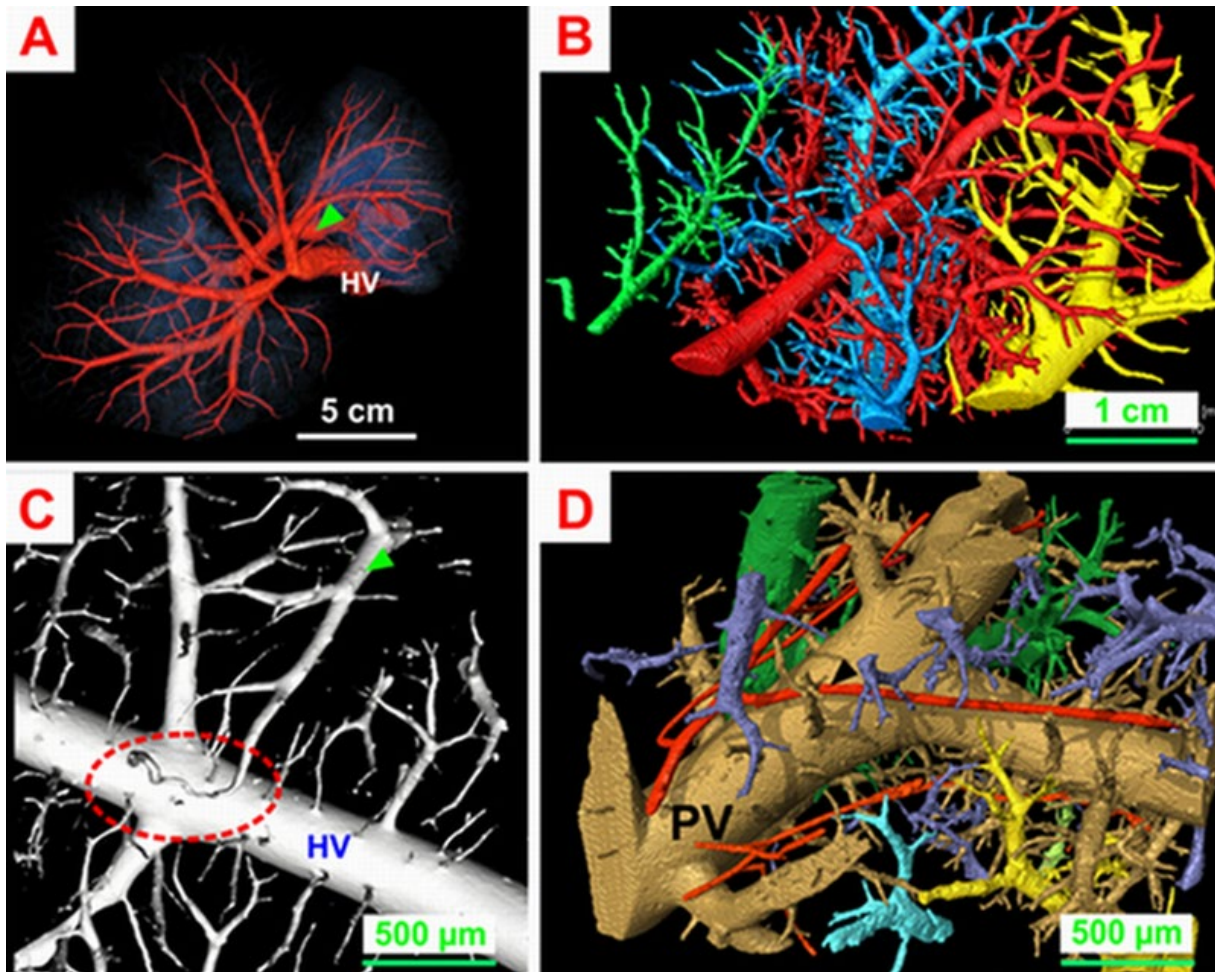


Fig. 2.

Computed tomography of porcine liver corrosion cast. (A) Macro-CT, VRT. Syntopic view of portal and hepatic venous systems; hepatic vein (HV), portal vein (green arrowhead). (B) μ -CT, 3-D reconstruction, cast filled via the portal vein. (C) μ -CT, volume rendering technique. Demonstration of porto-systemic anastomosis (red ellipse), tributary of hepatic portal vein (green arrowhead), and tributary of hepatic vein (HV). (D) μ -CT, 3-D reconstruction, cast filled via the portal vein (PV) and the hepatic artery (black arrowhead).

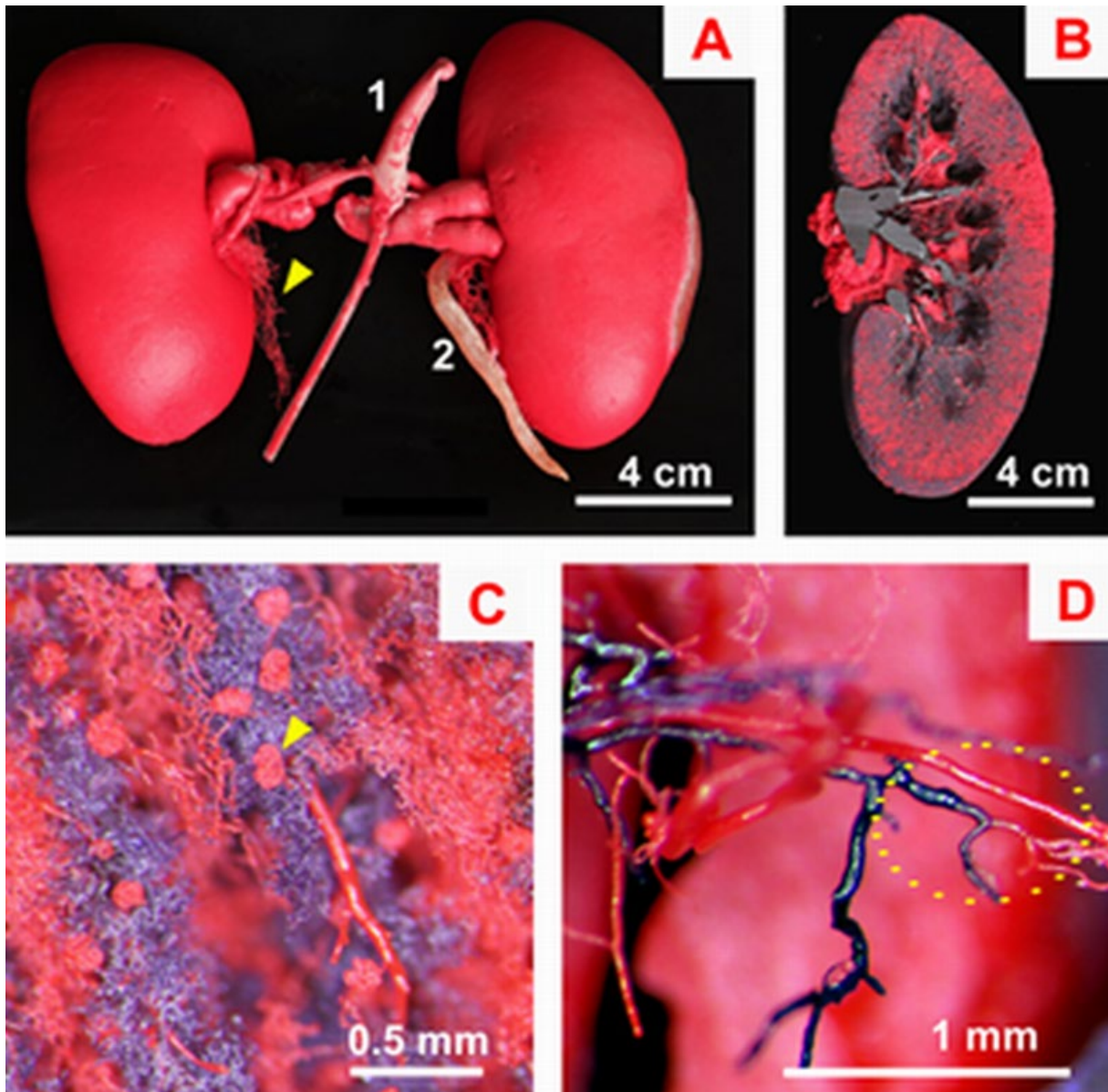


Fig. 3.

Pig kidney cast with Biodur E20[®] Plus. (A) Cast filled via the abdominal aorta (1), left kidney also via the ureter (2), ureteric branches (yellow arrowhead). (B, C, D) Filling via the renal artery (red) and the renal vein (blue). (B) Frontal section. (C) Renal cortex with glomerulus (yellow arrowhead). (D) Arterio-venous anastomosis (yellow ellipse).

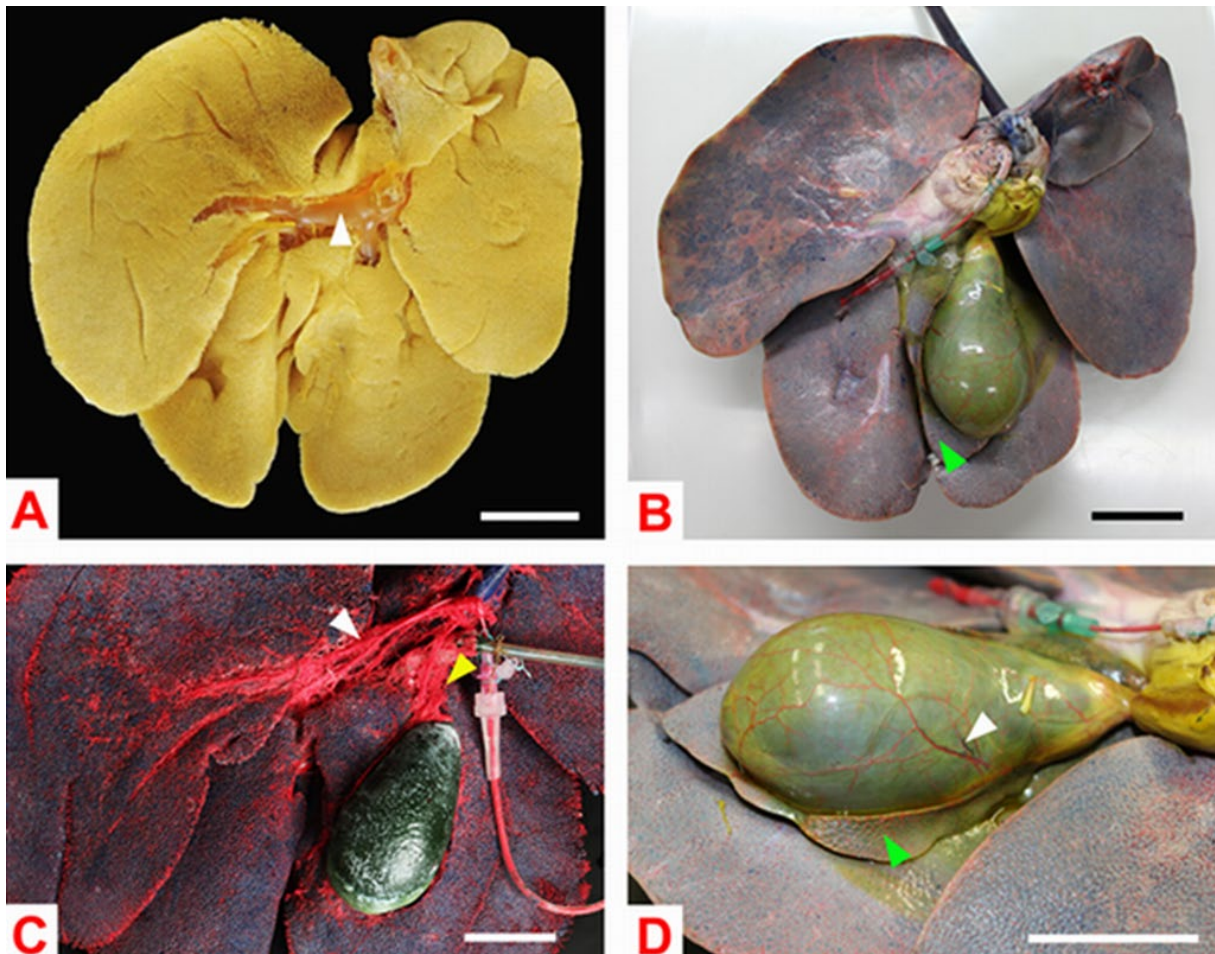


Fig. 1.

Corrosion casts of pig liver. (A) Filling with yellow-colored Biodur E20[®] Plus via the hepatic portal vein (white arrowhead). (B, D) Casts of liver and gallbladder (uncorroded) filled via the hepatic artery (red) and portal vein (blue). Quadrate lobe (green arrowhead). (C) Liver cast (after corrosion). Note the vasa vasorum of the portal vein (white arrowhead) and vessels of cystic duct (yellow arrowhead). (D) Gall bladder with cystic artery and vein (white arrowhead), quadrate lobe (green arrowhead). Scale bars 4 cm.

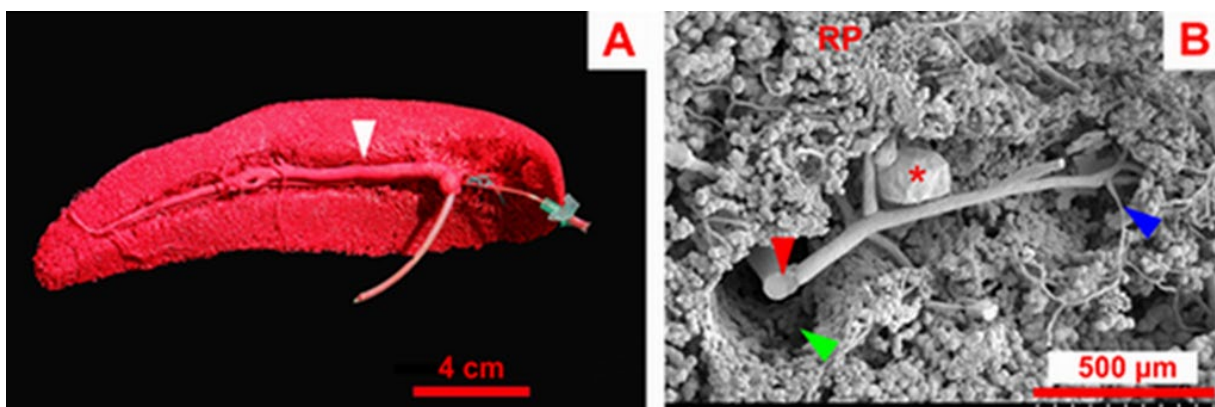


Fig. 5. Vascular corrosion cast of the porcine spleen. **(A)** Filling with red-colored Biodur E20[®] via the splenic artery and vein (white arrowhead). **(B)** SEM. Note central artery (red arrowhead), missing periarteriolar lymphatic sheath (green arrowhead), penicillar artery (blue arrowhead) and red pulp (RP). Asterisk marks extravasated Biodur.

Supplementary data – video.

μ -CT, 3-D reconstruction, pig liver corrosion cast filled via the portal vein (brown) and the hepatic artery (red).

Table 1
Resins suitable for corrosion casting

| <i>Group</i> | <i>Resin</i> | <i>Citation</i> | <i>Microvessel Permeability</i> | <i>Radiopacity</i> | <i>Official Price per Liter as of 1 April 2017</i> |
|-----------------------|------------------------------------|-------------------------------|---------------------------------|--------------------|----------------------------------------------------|
| <i>Acrylic Resins</i> | Mercocox Cl-2B | Lametschwandtner et al., 2004 | yes | yes | out of product. |
| | Mercocox II kit | Eberlova et al., 2015 | yes | yes | €777 |
| | Batson's #17 kit | Debbaut et al., 2014 | yes | yes | €329 |
| <i>Epoxy Resins</i> | Biodur E20® Plus | Eberlova et al., 2015 | yes | yes | €40 |
| <i>Polyurethanes</i> | Souda-foam® | De Sordi et al., 2014 | no | yes | €20 |
| | Polyurethane Elastomer (PU4ii) kit | Twelves et al., 2012 | no | yes | €954 |

Table 2

Porcine organs cast with Biodur E20® Plus

| <i>Organ</i> | <i>Method of Filling</i> | <i>Volume of Biodur E20® Plus</i> |
|-------------------------------|------------------------------------------|-----------------------------------|
| <i>Liver (N = 2)</i> | portal vein (MP) | 500 mL |
| <i>Liver (N = 2)</i> | portal vein (MP), hepatic artery (MMP) | 500 mL, 150 mL |
| <i>Liver (N = 1)</i> | portal vein (MP), hepatic artery (MMP) | 500 mL, 150 mL, 70 mL |
| <i>Spleen (N = 2)</i> | splenic artery (MMP) | 180 mL |
| <i>Spleen (N = 1)</i> | splenic artery (MMP), splenic vein (MMP) | 180 mL, 70 mL |
| <i>Kidney (N = 4)</i> | abdominal aorta (MP) | 300 mL |
| <i>Kidney (N = 2)</i> | renal artery (MMP), renal vein (MMP) | 130 mL, 70 mL |
| <i>Kidney (N = 1)</i> | renal artery (MMP), ureter (MP) | 130 mL, 70 mL |
| <i>Bronchial Tree (N = 2)</i> | trachea (MP) | 800 mL |

MP – manual pressure; **MMP** – micromanipulator; total number of animals, N = 7 (different combinations of organs were individually harvested)

Table 3
Schedule of elective anatomical classes

| | <i>Practical Session (150 min)</i> | <i>Subsequent Week Activities</i> | <i>Essential Student Aids</i> |
|---------------|------------------------------------|---------------------------------------|-----------------------------------------------------------------|
| <i>Week 1</i> | organ cannulating, resin injecting | cast hardening, corrosion, rinsing | protective glasses, lab coat, surgical gloves, respiratory mask |
| <i>Week 2</i> | stereomicroscopy, cast freezing | specimen cutting and cleaning for SEM | stereomicroscope |
| <i>Week 3</i> | scanning electron microscopy | | scanning electron microscope |

Table 4

Differences between porcine and human organs relevant for vascular corrosion casting

| <i>Organ (Pig)</i> | <i>Macroanatomy</i> | <i>Microanatomy</i> |
|--------------------------------|-----------------------------------------------------------------------------------------------------------------------------------------------------------------------------------------------------------------|-----------------------------------------------------------------------------------------------------------|
| <i>Liver</i> | right and left hemiliver divided by a deep fissure, 5 lobes (quadrate lobe is variable), caudal caval vein embedded in the right lateral and the caudate lobe, hilum more dorsally | each lobule is enveloped in fibrous connective tissue; fibrous tissue interconnect adjacent portal spaces |
| <i>Spleen</i> | elongated, strap-like; 2 segments, c.f., 4–5 segments in human spleen (Christo and DiDio, 1997) | |
| <i>Kidney</i> | upper and lower polar arteries at the hilum; 4 segments and 4 segmental arteries | |
| <i>Bronchial Tree and Lung</i> | 4 lobes in the right lung, right cranial lobar bronchus arises directly from the lateral wall of trachea; complete connective tissue septa border the secondary lobules; monopodial branching of bronchial tree | |

Table 5

Similarities between the porcine and human organs relevant for vascular corrosion casting

| <i>Organ (Pig)</i> | <i>Macroanatomy</i> | <i>Microanatomy</i> |
|---------------------------------------|-----------------------------------------------------------------------------------------------------------------------------------------------------------------------------|--------------------------------------------------------------------------------------------------------------------|
| <i>Liver</i> | similar size, hilum with PV, HA proper and right and left hepatic ducts; 8 segments | hepatic lobule, portal triad in portal spaces, sinusoids, central vein |
| <i>Spleen</i> | segmental arteries are end arteries | red pulp (vascular sinuses) and white pulp (central arteriole, periarteriolar lymphoid sheath, lymphoid follicles) |
| <i>Kidney</i> | similar size, smooth surface, medulla and cortex; renal pyramids, minor (approximately 10) and major (2–3) calices end in renal pelvis; segmental arteries are end arteries | renal corpuscle and convoluted tubules in cortex, straight tubules, loop of Henle and collecting ducts in medulla |
| <i>Bronchial Tree and Lung</i> | similar size; 2 lobes in the left lung | similar number of bronchial generations |